Fine-Tuning Blue-Emitting Halide Perovskite Nanocrystals

Stefan Martin, Nina A. Henke,* Carola Lampe, Markus Döblinger, Kilian Frank, Patrick Ganswindt, Bert Nickel, and Alexander S. Urban*

Lead halide perovskite nanocrystals (NCs) with narrow, bright emission in the visible range are promising candidates for light-emitting applications. Near-unity quantum yields have been realized for green and red-emitting perovskites, but efficient, stable blue-emitting perovskite materials are scarce. Current methods to synthesize quantum-confined $CsPbBr_3$ NCs with blue emission are limited to specific wavelength ranges and still suffer from inhomogeneously broadened emission profiles. Herein, anisotropic blue-green emitting $CsPbBr_3$ NCs are synthesized in ambient atmosphere using a spontaneous crystallization method. Optical spectroscopy reveals a gradual, asymptotic photoluminescence (PL) redshift of pristine colloidal NCs after synthesis. During this process, the emission quality improves notably as the PL spectra become narrower and more symmetric, accompanied by a PL intensity increase. Electron microscopy indicates that the gradual redshift stems from an isotropic growth of the $CsPbBr_3$ NCs in at least two dimensions, likely due to residual precursor ions in the dispersion. Most importantly, the growth process can be halted at any point by injecting an enhancement solution containing $PbBr_2$ and organic capping ligands. Thus, excellent control over NC size is achieved, allowing for nanometer-precise tunability of the respective emission wavelength in the range between 475 and 500 nm, enhancing the functionality of these already impressive NCs.

1. Introduction

Lead halide perovskite nanocrystals (NCs) were first reported in 2014, attracting much attention for optoelectronic applications, including solar cells, photodetectors, lasers, and light-emitting diodes (LEDs).[1–4] A narrow and tunable emission in the visible spectrum with near-unity quantum yields in colloidal dispersion and thin films established them as promising candidates for light-emitting applications.[5,6] Perovskite NCs have been successfully integrated into functioning LEDs, but limited stability and especially a low efficiency in the blue spectral range still hinder their widespread commercialization.[7,8] Typically, the halide component controls the emission wavelength; however, including chloride, which is necessary to obtain blue emission, renders the perovskite highly defect-prone.[8–10] Moreover, mixed-halide perovskites tend to undergo halide phase segregation, thus notably altering the emission output during device operation.[11,12] A promising approach for obtaining blue luminescence is reducing the size of perovskite NCs to the quantum confinement regime, analogous to conventional semiconductor quantum dots (QDs).[13–16] Moreover, an anisotropic size reduction, leading to, e.g., quasi-2D $CsPbBr_3$ nanoplatelets (NPLs) or quasi-1D nanowires/nanorods (NRs), has the additional benefit of enabling directional emission, potentially enhancing the outcoupling and boosting the theoretical maximum external quantum efficiencies (EQE) up to 28%.[17–23] While the quality of anisotropic perovskite NCs has improved significantly, blue-green photoluminescence (PL) spectra between 470 and 510 nm are still broader, owing to nonhomogeneous NC sizes in the confinement dimension. Most importantly, the precise emission color of $CsPbBr_3$ NPLs is limited to specific wavelengths, as the thickness is given in increments of octahedral monolayers (MLs).[21,24]

This work presents a room temperature (RT) synthesis of monodisperse, anisotropic $CsPbBr_3$ NCs with bright emission tunable with nanometric precision between 475 and 500 nm. As-prepared perovskite NCs initially show blueish PL at 475 nm but exhibit a slow, asymptotic redshift to the blue-green spectral range around 500 nm after synthesis. Significantly, the redshift can be halted at any time or desired emission maximum by treating the NCs with an enhancement solution containing $PbBr_2$, oleylamine, and oleic acid ligands, as detailed previously.[21] The

S. Martin, N. A. Henke, C. Lampe, P. Ganswindt, A. S. Urban
Nanospectroscopy Group and Center for NanoScience
Nano-Institute Munich
Faculty of Physics
Ludwig-Maximilians-University Munich
80539 Munich, Germany
E-mail: Nina.Henke@physik.uni-muenchen.de; urban@lmu.de
M. Döblinger
Department of Chemistry
Ludwig-Maximilians-University Munich
81377 Munich, Germany
K. Frank, B. Nickel
Soft Condensed Matter Group and Center for NanoScience
Faculty of Physics Ludwig-Maximilians-University Munich
80539 Munich, Germany

**ADVANCED
SCIENCE NEWS**

www.advancedsciencenews.com

**ADVANCED
OPTICAL
MATERIALS**
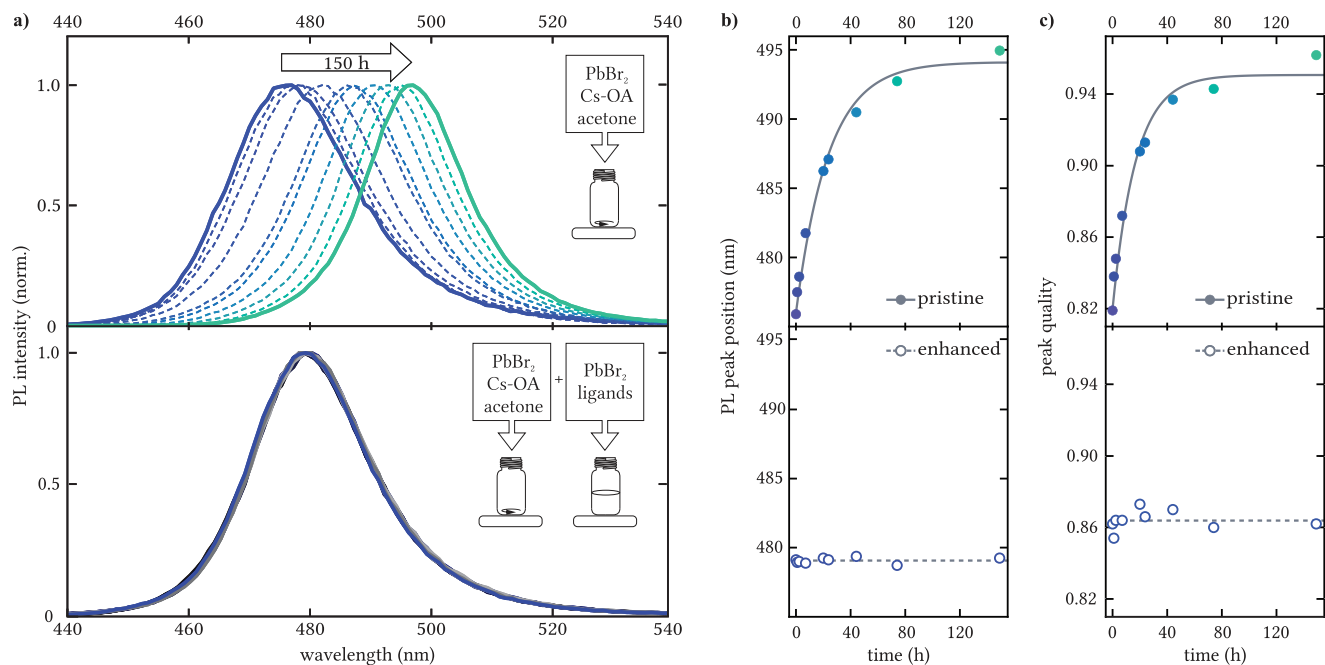
www.advopticalmat.de

Figure 1. a) Steady-state PL spectra of CsPbBr₃ NCs measured over 150 h after synthesis. Evolution of b) PL peak position and c) peak quality factor of as-synthesized (top) and enhanced NC dispersions (bottom) within 150 h after synthesis.

emission profiles of the so-obtained NCs remain stable for at least several weeks. The PL emission is spectrally tunable and improves substantially over time during the redshift as the quantum yield (QY) increases, and the linewidth decreases. Electron microscopy confirms that the asymptotic redshift of the PL emission results from a 2D proportional growth of perovskite NCs after synthesis. Summarily, this work constitutes a new strategy to exploit postsynthetic evolution in quantum-confined anisotropic NCs for achieving better color tunability in wavelength ranges that have not yet been explored as extensively or are not easily accessible by direct synthesis.

2. Results and Discussion

The presented synthesis is based on the ligand-assisted spontaneous crystallization of NCs in nonpolar organic solvents.[21] Unlike standard hot-injection procedures for synthesizing lead halide perovskite NCs which require high reaction temperatures and an inert gas atmosphere,[25] our synthesis is conducted at RT in an ambient atmosphere. Cesium-oleate is injected into a precursor solution of PbBr₂, oleic acid, and oleylamine ligands in toluene. Acetone is added to promote NC formation and precipitation, acting as an antisolvent. After stirring for 60 s, the reaction is terminated by centrifugation. The supernatant is discarded, and the precipitate of CsPbBr₃ NCs is redispersed in n-hexane. A deficit of Cs⁺ ions compared to available Pb²⁺ ions restricts crystal growth, thus promoting the formation of anisotropic quasi-2D perovskite NPLs, whose thickness can be controlled from 2 to 8MLs through the Cs:Pb ratio.[17,21,24] Subsequently, an enhancement solution comprising PbBr₂ and organic capping ligands in hexane is added to repair surface defects stemming from lead and

bromide vacancies in the NCs, enhancing their overall PLQY and stability.[21]

Using a Cs:Pb ratio of 0.56, we synthesized CsPbBr₃ NCs with sky-blue emission centered at 475 nm, corresponding to the PL of 4ML NPLs.[26] To investigate the long-term stability and potential degradation pathways of unpassivated NCs, we did not add the enhancement solution in contrast to the normal synthesis. For this, we recorded steady-state PL spectra at intervals up to 150 h after the synthesis. Surprisingly, the PL spectrum gradually redshifts throughout the measurement (**Figure 1**a, top). This starkly contrasts the standard sample, which shows no change in the PL spectrum over the same 150 h (Figure 1a, bottom). As shown in Figure 1b (top), the redshift is relatively rapid at the beginning, shifting by over 10 nm in the first 20 h, but it swiftly decelerates over time, demonstrating an asymptotic behavior according to Equation 1

$$y = a \cdot (1 - \exp(-b \cdot t)) \qquad (1)$$

Here, a denotes the asymptotic limit of the redshift, and b is the shift velocity. As explained, the passivated NCs do not show any variation in the PL emission maximum over time (Figure 1, bottom). We note that at $t = 0$ the emission maximum of the passivated sample is redshifted by 2 nm compared to the unpassivated sample, a reproducible effect which we attribute to the slight increase in NC size and a change in the dielectric surrounding upon the addition of the enhancement solution.[13,27,28] Often, a redshift or the emergence of secondary peaks in the PL of NC dispersions signifies a loss of colloidal stability accompanied by aggregation of individual NCs and worse optical properties. Especially anisotropic NCs with high surface-to-volume ratios tend to aggregate and coalesce readily, thus forming larger perovskite

**ADVANCED
SCIENCE NEWS**

www.advancedsciencenews.com

**ADVANCED
OPTICAL
MATERIALS**

www.advopticalmat.de

crystals in which excitons experience weaker confinement.[29–32] However, neither additional peaks nor shoulders that could be attributed to the coincidental formation of thicker NPLs or bulk-like NCs were observed, suggesting a highly uniform size distribution of anisotropic perovskite NCs, as confirmed by respective TEM images (Figure S1, Supporting Information). To further investigate the cause of the redshift in our case, we derive a peak quality factor, assessing the optical quality of the NC dispersions through their PL spectra. The peak quality factor f_{PL} is calculated from contributions of the peak symmetry, skewness and width, overall assigning a value between 0 and 1, with 1 signifying an optimal spectrum. A detailed derivation of f_{PL} is included in the experimental section. The PLQY of the sample is not factored into the calculation of f_{PL}, as it does not provide information on colloidal stability and is discussed later.

The enhanced NCs exhibit a value around $f_{PL} = 0.86$ which stays essentially constant over the 150 h after synthesis (Figure 1c, bottom). The PL spectra being very symmetric and narrow ($FWHM = 23$ nm) signifies a high quality of the NCs. Likewise, the PL peak position of enhanced NCs is stable for at least 150 h (Figure 1b, bottom). However, instead of becoming worse, the optical quality of pristine NC dispersions continuously improves as f_{PL} increases from 0.82 to 0.96 (Figure 1c, top). The predominant contribution stems from the narrowing of the emission profile ($FWHM \approx 19$ nm after 150 h), but the peak symmetry improves as well (Figure S2, Supporting Information). Interestingly, the development of f_{PL} is accurately described by the same function given in Equation 1, suggesting a correlation between peak position and quality. The redshift is not due to an aggregation or degradation of NCs, but more likely signifies a gradual size increase and a focusing of the overall size of the NCs around an optimal value. This narrowing is astounding as thicker CsPbBr$_3$ NPLs typically exhibit less narrow spectra, likely due to a higher polydispersity in the strong confinement dimension.[24]

An important question, especially for applications, is whether adding an enhancement solution can terminate the PL redshift at any point during the synthesis. We repeated the synthesis of CsPbBr$_3$ NCs, splitting the colloidal dispersion into seven separate aliquots, and diluted them slightly for subsequent optical characterization. The samples were stored in darkness under ambient conditions, and each aliquot was treated with enhancement solution after a varying delay time, ranging from 0 to 150 h. Steady-state absorbance and PL spectra of each aliquot were acquired individually after treatment with an enhancement solution (**Figure 2**). With a longer delay between synthesis and enhancement, excitonic absorption and PL of individual aliquots continuously shift to longer wavelengths before being halted by adding an enhancement solution. After 150 h, the absorption peak of the last NC aliquot shifted from 460 to 478 nm, while the PL shifted from 478 to 496 nm before enhancement was added. Subsequently, no further changes were observed for any of the seven aliquots, and the enhanced NC dispersions' emission profiles remained stable for at least 15 more days (Figure 2b). The overall shift of 18 nm in both absorption and PL is comparable with a transition from 4ML to 6ML CsPbBr$_3$ NPLs, and the gradual absorption and emission shift to lower energies as well as the less prominent appearance of excitonic absorption suggest a weaker confinement in ripened CsPbBr$_3$ NCs. As before, the peak position and quality factor follow the same asymptotic

trend depicted in Figure 1b,c, emphasizing the reproducibility of the postsynthetic shift. Additionally, the PL intensity increased by 5% upon enhancement for all aliquots. Overall, this demonstrates how adding enhancement solution to colloidal CsPbBr$_3$ NCs can effectively halt the post-synthesis PL redshift at any point, thereby achieving nanometer-precise emission tunability between 475 and 500 nm while also improving the color purity of the emitted light (Figure S3, Supporting Information). Moreover, the PL stability of enhanced perovskite NCs is maintained in thin films (Figure S4, Supporting Information), which is particularly important for potential device integration of perovskite NCs.

To confirm that the perovskite lattice is conserved during all stages of the post-synthetic PL redshift and subsequent enhancement, we performed powder X-ray diffraction (XRD) measurements of pristine NCs as well as of NCs enhanced after different delay times. The perovskite crystal structure is maintained, and the characteristic peak broadening of few-nanometer-sized NCs was observed for all samples, as confirmed by the XRD data and refinement (Figure S5, Supporting Information). Considering all results, we determine that the perovskite NCs undergo a controlled growth in size rather than an arbitrary aggregation and coalescence since none of the acquired spectra indicate a coexistence of two or more different NC populations. To verify this assumption, we need to look at individual NCs directly, necessitating the use of an electron microscope, given the small size of the NCs. To this end, we modified the synthesis to obtain two CsPbBr$_3$ NC dispersions with a different initial emission wavelength and repeated the measurements. This time, we separated the samples into two aliquots each, terminating the PL redshift immediately in one case and after 120 h in the second case. The corresponding PL spectra, shown in **Figure 3**a, highlight the slightly redshifted initial PL emission maximum and a comparable redshift of the PL over 120 h. This shift correlates to a thickness increase from 4ML to 5ML in the one sample and 3.5ML to 4.5ML in the second sample, a result which initially seems puzzling, as 2D NPLs have not been shown to exhibit inter-ML thickness and luminescence features. To investigate this, we used a probe-corrected Titan Themis at 300 kV in high-angle annular dark-field scanning transmission electron microscopy (HAADF-STEM) mode to image these NCs (Figure 3b). These images and a fast Fourier transform (FFT) analysis of individual NCs reveal a d-spacing of 0.60 nm characteristic for either a cubic or orthorhombic perovskite lattice, confirming their expected halide perovskite nature (Figure S6, Supporting Information).[33] The observed NCs are quite regular in size, exhibiting two distinct dimensions that had been ascribed to the 2D NPLs stacking upright on the substrates.[21] As shown in Figure 3b, the NCs on the left are slightly larger than those on the right, matching the associated redshifted PL spectra. Additionally, both dispersions increase in NC size during the 120 h before the passivation of the second aliquot. Notably, a 2D homogeneous size increase is observed for both samples by $\approx$25% from 3.4 nm x 11.2 nm to 4.3 nm x 13.9 nm (left) and from 3.2 nm x 11.5 nm to 3.8 nm x 14.8 nm (right). The large dimension for both samples is in the weakly to nonconfined regime. Accordingly, the smaller dimension governs the spectral position of the optical resonances. The apparent thickness of perovskite NCs observed in the HAADF-STEM images corresponds roughly to a size increase from 6ML
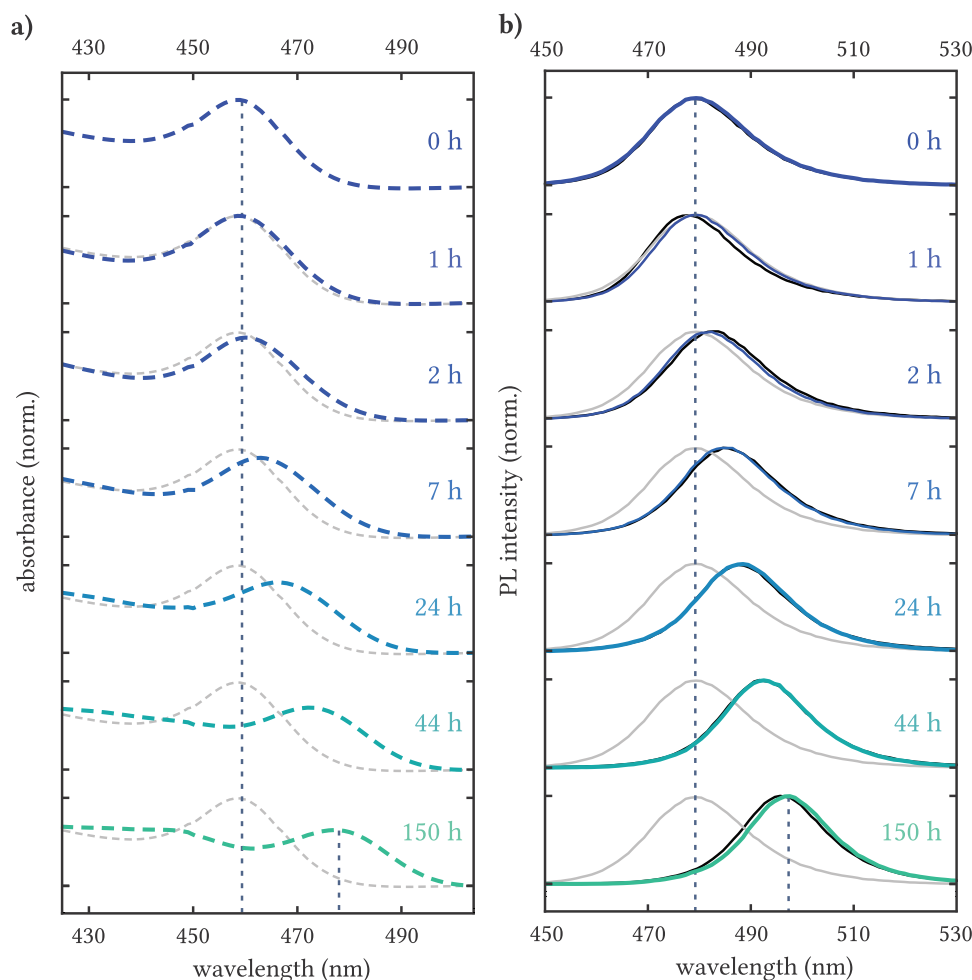
**ADVANCED
SCIENCE NEWS**

www.advancedsciencenews.com

**ADVANCED
OPTICAL
MATERIALS**

www.advopticalmat.de

Figure 2. a) Absorbance and b) PL spectra of enhanced CsPbBr$_3$ NCs from the same synthesis batch. The delay between synthesis and enhancement was varied between 0 and 150 h, thus terminating the redshifting process at different points and resulting in concomitantly redshifting emission wavelengths. Spectra were acquired immediately after synthesis (grey), 150 h after synthesis (color), and 20 d after synthesis (black).

to 7ML and 5ML to 6ML for the two samples. Additionally, the NCs have a well-defined asymmetric shape, but we cannot confirm whether they are as supposed 2D NPLs or quasi-1D NRs as observed in other studies. Nevertheless, their behavior can be regarded as quasi-1D.[34,35] Notwithstanding, we observe a proportional growth of NCs in two dimensions which adequately explains the gradual redshift of the corresponding emission profile.

We theorize that growth proceeds by incorporating residual precursor material from the synthesis, particularly Cs-oleate. As-synthesized perovskite NCs are often not sufficiently passivated with oleylamine and oleic acid, exhibiting highly dynamic ligand binding and poor colloidal stability.[36,37] Therefore, excess Cs-oleate or PbBr$_2$ in colloidal dispersions can initiate classical growth of perovskite NCs after synthesis. As the concentration of available precursor material becomes depleted, the growth rate and PL shift slow down significantly and eventually terminate. This presumption is also supported by the observation that reducing the Cs-oleate concentration in the synthesis substantially decreases the post-synthetic shift of the PL peak wavelength in pristine samples (Figure S7, Supporting Information). Treatment with an enhancement solution passivates the perovskite

surface and improves the surrounding ligand shell, thus effectively preventing further growth, as oleylammonium (OlAm$^+$) directly competes with Cs$^+$ ions for the same lattice position on the perovskite surface.[38] A nonclassical growth mechanism by oriented attachment was considered; however, this implies a distinct, stepwise increase of perovskite NC size through the coalescence of multiple particles, which does not align with the NC sizes in Figure 3b.[39,40] As a final piece of the puzzle, we calculated the relative PLQY of enhanced samples from Figure 2, analyzing the correlation with the NCs' emission wavelength and comparing it to the peak quality factor f_{PL} (**Figure 4**). For this purpose, the integrated emission intensity was divided by the optical density at the excitation wavelength and then normalized with respect to the aliquot enhanced immediately after synthesis. The peak quality increases linearly with the emission wavelength of CsPbBr$_3$ NCs while the relative PLQY drops to 0.55 within two hours after synthesis, at an emission wavelength of 482 nm, but then increases steadily, almost reaching its initial value after 150 h.

Assuming a classical growth of colloidal NCs from precursor material, this could be interpreted as follows. The nucleation of
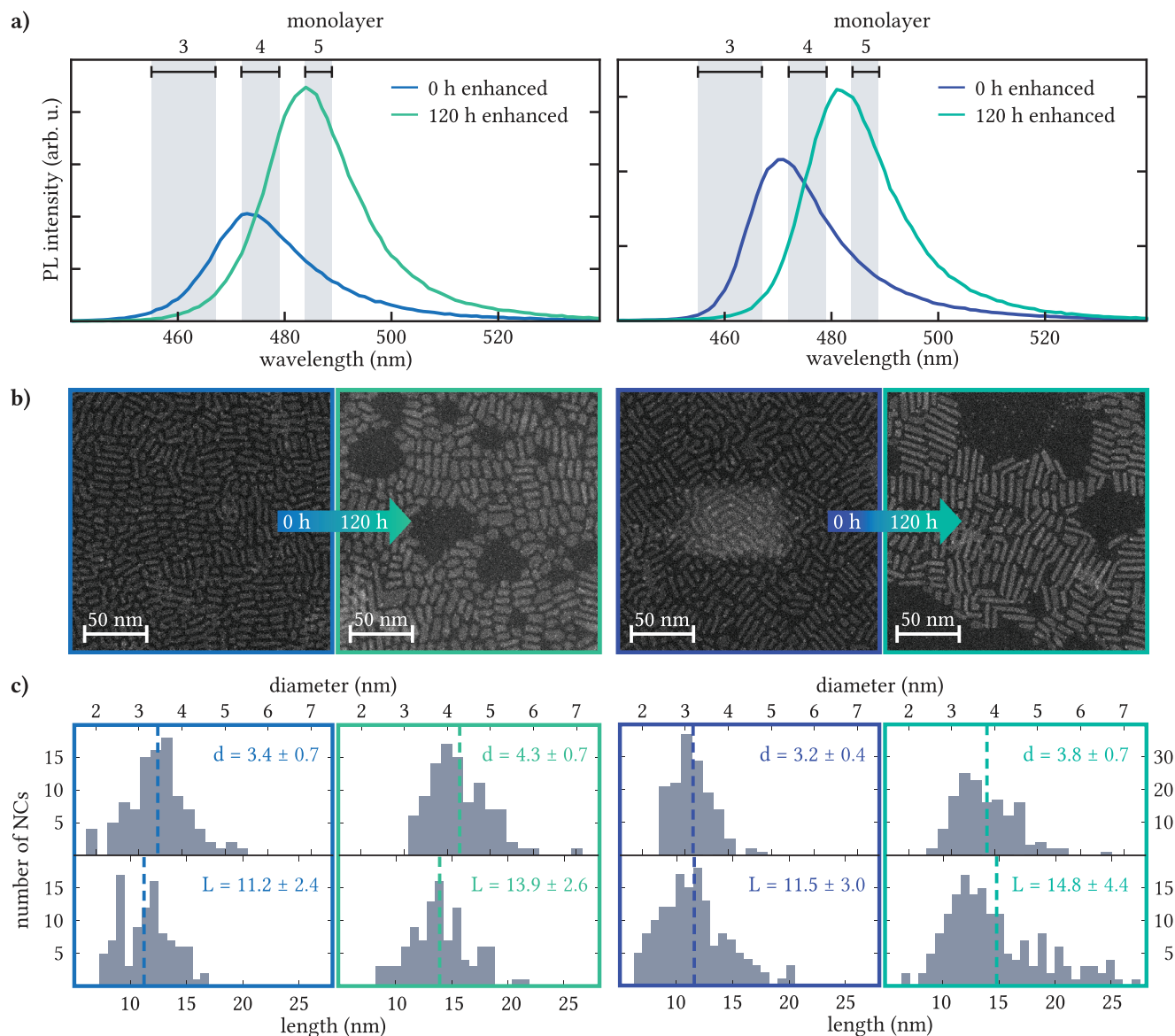
ADVANCED
SCIENCE NEWS

www.advancedsciencenews.com

ADVANCED
OPTICAL
MATERIALS

www.advopticalmat.de

Figure 3. a) PL spectra and b) HAADF-STEM images of CsPbBr3 NCs with different sizes and, consequently, emission wavelengths. The NC samples were obtained from two different syntheses, with one sample shifting from emitting at 473–485 nm (left) and the other from 471 to 481 nm (right) within 120 h. Grey areas indicate the emission range of 3ML, 4ML, and 5ML NPLs. c) Distribution of NC diameter d and length L. Dashed lines in the histograms mark the average value.

incomplete crystal layers on the surface of existing perovskite NCs with residual precursor ions in the dispersion temporarily leads to a higher surface-to-volume ratio, creating more trap states and enhancing nonradiative recombination.[21,41–43] This is supported by HAADF-STEM images of individual CsPbBr$_3$ NCs with the lowest relative PLQY of 0.55, which show multiple NCs with irregular crystal shapes (see Figure S8 in the Supporting Information). However, as new layers continue expanding and ultimately encompass the entire NC, the relative PLQY recovers steadily and approximately reaches its initial value. Moreover, due to surface energetics, it is more likely that partial layers will be completed rather than that new ones will be started, which

explains the narrowing of the optical spectra due to higher NC homogeneity. Overall, the color purity and wavelength tunability of presented anisotropic CsPbBr$_3$ NCs is superior to those of comparable blue-green emitting CsPbBr$_3$ NPLs obtained from a direct synthesis.

3. Conclusion

In summary, we have shown how to obtain narrow blue-green emission tunable with nanometer-precision from anisotropic CsPbBr$_3$ NCs by controlling their postsynthetic growth. Due to lower colloidal stability, as-synthesized perovskite NCs exhibit
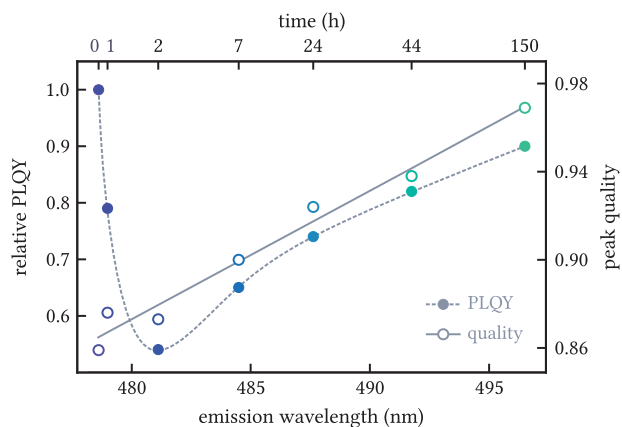
**ADVANCED
SCIENCE NEWS**

www.advancedsciencenews.com

**ADVANCED
OPTICAL
MATERIALS**

www.advopticalmat.de

Figure 4. Evolution of relative PLQY and peak quality depending on the emission wavelength of colloidal CsPbBr$_3$ NCs.

an asymptotic redshift of absorption and emission features over seven days after synthesis. We attribute the gradual shift to a slow, 2D proportional growth of CsPbBr$_3$ NCs, most likely from excess precursor material in the colloidal dispersions, particularly Cs-oleate. During this process, the PL profiles become narrower and more symmetric, and the PL intensity increases, notably improving the emission peak quality. Most importantly, the growth can be halted at any point by passivating the NC surface with an enhancement solution containing PbBr$_2$ and additional organic capping ligands. Perovskite NCs obtained by this method are stable for several weeks in colloidal dispersion and thin films and show superior emission color purity compared to 4–6ML NPLs obtained from a direct RT synthesis. Electron microscopy reveals a 2D proportional growth, suggesting that these NCs are more akin to 1D NRs than 2D NPLs. Controlling postsynthetic growth in quantum-confined perovskite NCs should be explored for emission fine-tuning in wavelength ranges that are not as easily accessible by conventional synthesis methods, i.e., deep-blue or yellow emission, thereby greatly enhancing the applicability of these fascinating NCs. Future research should also focus on controlling the precise orientation of blue-green emitting anisotropic NCs in thin films and optimizing their absolute PLQY and long-term stability in the film state, thus exploiting their vast potential for a bright, directional blue-green emission.

4. Experimental Section

Materials: Cs$_2$CO$_3$ (cesium carbonate, 99%), PbBr$_2$ (lead (II) bromide, $\geq$ 98%), oleic acid (technical grade, 90%), and oleylamine (technical grade, 70%) were purchased from Sigma Aldrich. Toluene (for HPLC, >99%), *n*-hexane (for HPLC, >97%), and acetone (for HPLC, >99.9%) were purchased from VWR Chemicals. All chemicals were used without further purification.

Synthesis of Anisotropic CsPbBr$_3$ Nanocrystals: The Cs-oleate precursor was prepared by dissolving Cs$_2$CO$_3$ (0.1 mmol, 32.5 mg) in oleic acid (10 mL) under stirring at 85 °C for up to three hours until a clear solution was obtained. The PbBr$_2$-precursor was prepared by dissolving PbBr$_2$ (0.1 mmol, 36.7 mg) in toluene (10 mL), oleic acid, and oleylamine (100 µL each) under stirring at 85 °C for up to three hours until a clear solution is obtained. The PbBr$_2$-enhancement solution was prepared by dissolving PbBr$_2$ (0.1 mmol, 36.7 mg) in *n*-hexane (10 mL), oleic acid, and oleylamine (100 µL each) in the same manner. The synthesis

of anisotropic CsPbBr$_3$ NCs is carried out at RT (20–22 °C) in ambient atmosphere (30–40% humidity). Cs-oleate precursor (504 µL) is added to PbBr$_2$-precursor (1794 µL) in a glass vial under vigorous stirring. After 10 s, acetone (3702 µL) is added to initiate the formation and precipitation of perovskite NCs. The reaction mixture is stirred for 60 s and then centrifuged at 4000 rpm (*Hettich Rotina 380R*, 117 mm) for 3 min. The supernatant is discarded, and the precipitate is redispersed in *n*-hexane (4 mL). To enhance colloidal perovskite NCs, 400 µL (or 10% vol) of the PbBr$_2$-enhancement solution is added to improve NC stability and emission properties.

Thin Film Preparation: Thin films of perovskite NCs were prepared by drop casting 100 µL of a colloidal NC dispersion in hexane on a 15×15 mm borosilicate glass substrate. Before drop casting, the glass substrates were cleaned by ultrasonication in acetone and isopropanol and dried under a nitrogen stream.

Optical Characterization: Absorbance and photoluminescence spectra were measured on a commercial *FluoroMax-4Plus* spectrometer equipped with a xenon arc lamp and an F-3031 transmission accessory (*HORIBA Scientific*). The excitation wavelength for photoluminescence spectra was set to 400 nm. Colloidal samples were analyzed in quartz cuvettes (*Hellma Analytics*).

Morphological Characterization: STEM-HAADF mode was performed with a probe-corrected *Titan Themis (FEI)* at an acceleration voltage of 300 kV. TEM imaging at lower magnifications was performed on a JOEL *JEM-1100* microscope operated at an acceleration voltage of 80 kV.

Structural Characterization: X-ray powder diffraction data were taken of samples drop-casted onto a single layer of adhesive tape (*3 M Scotch Magic 810*, 10×5 µL) with molybdenum Kα radiation ($\lambda = 0.71$ Å) in transmission mode. A Pilatus 100K (*Dectris*) was used as a detector with a total measurement time of 3 h per sample.

Calculation of Peak Quality: The peak quality was assessed by combining two parameters, one for symmetry and one for the width of the emission profile, thereby reflecting the color purity of emitted light. First, the normalized emission peak was split into two halves, to the left and right of the peak maximum. The area of each half ($A_1 < A_2$) was calculated with a cumulated sum and then included in the area relation a_{rel} according to Equation 2

$$a_{rel} = \sqrt[3]{\frac{A_1}{A_2}} \tag{2}$$

Second, the skewness factor s was defined by Equation 3 from the half width half maximum of the peak profile on either side of the maximum position ($hwhm_1 < hwhm_2$)

$$s = \sqrt[3]{\frac{hwhm_1}{hwhm_2}} \tag{3}$$

These two components were combined in the symmetry factor f_{sym} given in Equation 4

$$f_{sym} = \sqrt{a_{rel} \cdot s} \tag{4}$$

To calculate the width factor f_{width}, the full-width at half-maximum $fwhm_{eV}$ was corrected according to Equation 5. The contribution of peak width to f_{width} depends on the position of the peak maximum c_{eV}, allowing peak profiles of lower energy emission to adopt higher values of $fwhm_{eV}$ without resulting in a higher width factor f_{width} derived from Equation 6

$$fwhm_{corr} = fwhm_{eV} - ((c_{eV} - 2.4 \text{ eV}) \times (-0.00905)) \tag{5}$$

$$f_{width} = -6.9 \text{ eV}^{-1} \times fwhm_{corr} + 1.7 \tag{6}$$

**ADVANCED
SCIENCE NEWS**

www.advancedsciencenews.com

**ADVANCED
OPTICAL
MATERIALS**

www.advopticalmat.de

Both parameters were combined to calculate the overall peak quality factor f_{PL} in Equation 7

$$f_{PL} = \sqrt[3]{f_{width} \times f_{sym}^2} \qquad (7)$$

Accordingly, f_{PL} adopts values between 0 and 1. Broad and asymmetric emission peaks are rated with a value approaching 0 (low quality), whereas very narrow, symmetric peaks are assigned a value close to 1 (high quality).

Supporting Information

Supporting Information is available from the Wiley Online Library or from the author.

Conflict of Interest

The authors declare no conflict of interest.

Data Availability Statement

The data that support the findings of this study are available from the corresponding author upon reasonable request.

[1] L. C. Schmidt, A. Pertegas, S. Gonzalez-Carrero, O. Malinkiewicz, S. Agouram, G. M. Espallargas, H. J. Bolink, R. E. Galian, J. Perez-Prieto, *J. Am. Chem. Soc.* **2014**, *136*, 850.

[2] Y. T. Huang, S. R. Kavanagh, D. O. Scanlon, A. Walsh, R. L. Z. Hoye, *Nanotechnology* **2021**, *32*, 132004.

[3] A. Dey, J. Ye, A. De, E. Debroye, S. K. Ha, E. Bladt, A. S. Kshirsagar, Z. Wang, J. Yin, Y. Wang, L. N. Quan, F. Yan, M. Gao, X. Li, J. Shamsi, T. Debnath, M. Cao, M. A. Scheel, S. Kumar, J. A. Steele, M. Gerhard, L. Chouhan, K. Xu, X.-g. Wu, Y. Li, Y. Zhang, A. Dutta, C. Han, I. Vincon, A. L. Rogach, et al., *ACS Nano* **2021**, *15*, 10775.

[4] J. Zhang, Q. Wang, X. Zhang, J. Jiang, Z. Gao, Z. Jin, S. Liu, *RSC Adv.* **2017**, *7*, 36722.

[5] J. Shamsi, A. S. Urban, M. Imran, L. De Trizio, L. Manna, *Chem. Rev.* **2019**, *119*, 3296.

[6] S. Kar, N. F. Jamaludin, N. Yantara, S. G. Mhaisalkar, W. L. Leong, *Nanophotonics-Berlin* **2021**, *10*, 2103.

[7] G. Schileo, G. Grancini, *J. Mater. Chem. C* **2021**, *9*, 67.

[8] P. Du, L. Gao, J. Tang, *Front. Optoelectron.* **2020**, *13*, 235.

[9] D. P. Nenon, K. Pressler, J. Kang, B. A. Koscher, J. H. Olshansky, W. T. Osowiecki, M. A. Koc, L. W. Wang, A. P. Alivisatos, *J. Am. Chem. Soc.* **2018**, *140*, 17760.

[10] J. Ye, M. M. Byranvand, C. O. Martinez, R. L. Z. Hoye, M. Saliba, L. Polavarapu, *Angew. Chem., Int. Ed. Engl.* **2021**, *60*, 21636.

[11] M. C. Brennan, S. Draguta, P. V. Kamat, M. Kuno, *ACS Energy Lett.* **2017**, *3*, 204.

[12] H. Zhang, X. Fu, Y. Tang, H. Wang, C. Zhang, W. W. Yu, X. Wang, Y. Zhang, M. Xiao, *Nat. Commun.* **2019**, *10*, 1088.

[13] A. L. Efros, L. E. Brus, *ACS Nano* **2021**, *15*, 6192.

[14] J. B. N. D. J. Murray, M. G. Bawendi, *J. Am. Chem. Soc.* **1993**, *115*, 8706.

[15] Q. A. Akkerman, T. P. T. Nguyen, S. C. Boehme, F. Montanarella, D. N. Dirin, P. Wechsler, F. Beiglböck, G. Rainò, C. Erni, C. Katan, J. Even, M. V. Kovalenko, *Science* **2022**, *377*, 1406.

[16] Q. A. Akkerman, *Nano Lett.* **2022**, *22*, 8168.

[17] C. Otero-Martinez, J. Ye, J. Sung, I. Pastoriza-Santos, J. Perez-Juste, Z. Xia, A. Rao, R. L. Z. Hoye, L. Polavarapu, *Adv. Mater.* **2022**, *34*, 2107105.

[18] D. Zhang, Q. Zhang, Y. Zhu, S. Poddar, Y. Zhang, L. Gu, H. Zeng, Z. Fan, *Adv. Energy Mater.* **2022**, 2201735.

[19] D. Zhang, Y. Yu, Y. Bekenstein, A. B. Wong, A. P. Alivisatos, P. Yang, *J. Am. Chem. Soc.* **2016**, *138*, 13155.

[20] D. Yang, P. Li, Y. Zou, M. Cao, H. Hu, Q. Zhong, J. Hu, B. Sun, S. Duhm, Y. Xu, Q. Zhang, *Chem. Mater.* **2019**, *31*, 1575.

[21] B. J. Bohn, Y. Tong, M. Gramlich, M. L. Lai, M. Döblinger, K. Wang, R. L. Z. Hoye, P. Müller-Buschbaum, S. D. Stranks, A. S. Urban, L. Polavarapu, J. Feldmann, *Nano Lett.* **2018**, *18*, 5231.

[22] T. Morgenstern, C. Lampe, T. Naujoks, M. Jurow, Y. Liu, A. S. Urban, W. Brütting, *J. Lumin.* **2020**, *220*, 116939.

[23] M. J. Jurow, T. Morgenstern, C. Eisler, J. Kang, E. Penzo, M. Do, M. Engelmayer, W. T. Osowiecki, Y. Bekenstein, C. Tassone, L.-W. Wang, A. P. Alivisatos, W. Brütting, Y. Liu, *Nano Lett.* **2019**, *19*, 2489.

[24] C. Lampe, I. Kouroudis, M. Harth, S. Martin, A. Gagliardi, A. S. Urban, *Adv. Mater.* **2023**, *35*, 2208772.

[25] L. Protesescu, S. Yakunin, M. I. Bodnarchuk, F. Krieg, R. Caputo, C. H. Hendon, R. X. Yang, A. Walsh, M. V. Kovalenko, *Nano Lett.* **2015**, *15*, 3692.

[26] M. Gramlich, M. W. Swift, C. Lampe, J. L. Lyons, M. Doblinger, A. L. Efros, P. C. Sercel, A. S. Urban, *Adv. Sci.* **2022**, *9*, 2103013.

[27] A. V. Rodina, A. L. Efros, *J. Exp. Theor. Phys.* **2016**, *122*, 554.

[28] J. T. Lin, C. C. Liao, C. S. Hsu, D. G. Chen, H. M. Chen, M. K. Tsai, P. T. Chou, C. W. Chiu, *J. Am. Chem. Soc.* **2019**, *141*, 10324.

[29] Y. Wang, X. Li, S. Sreejith, F. Cao, Z. Wang, M. C. Stuparu, H. Zeng, H. Sun, *Adv. Mater.* **2016**, *28*, 10637.

[30] M. C. Weidman, A. J. Goodman, W. A. Tisdale, *Chem. Mater.* **2017**, *29*, 5019.

[31] J. Shamsi, D. Kubicki, M. Anaya, Y. Liu, K. Ji, K. Frohna, C. P. Grey, R. H. Friend, S. D. Stranks, *ACS Energy Lett.* **2020**, *5*, 1900.

[32] H. Liu, M. Worku, A. Mondal, T. B. Shonde, M. Chaaban, A. Ben-Akacha, S. Lee, F. Gonzalez, O. Olasupo, X. Lin, J. S. R. Vellore Winfred, Y. Xin, E. Lochner, B. Ma, *Adv. Energy Mater.* **2022**, 2201605.

[33] F. Bertolotti, G. Nedelcu, A. Vivani, A. Cervellino, N. Masciocchi, A. Guagliardi, M. V. Kovalenko, *ACS Nano* **2019**, *13*, 14294.

[34] E. Socie, B. R. C. Vale, A. T. Terpstra, M. A. Schiavon, J.-E. Moser, *J. Phys. Chem. C* **2021**, *125*, 14317.

[35] B. R. C. Vale, E. Socie, A. Burgos-Caminal, J. Bettini, M. A. Schiavon, J. E. Moser, *J. Phys. Chem. Lett.* **2020**, *11*, 387.

[36] J. De Roo, M. Ibáñez, P. Geiregat, G. Nedelcu, W. Walravens, J. Maes, J. C. Martins, I. Van Driessche, M. V. Kovalenko, Z. Hens, *ACS Nano* **2016**, *10*, 2071.

**ADVANCED
SCIENCE NEWS**

www.advancedsciencenews.com

**ADVANCED
OPTICAL
MATERIALS**

www.advopticalmat.de

[37] M. I. Bodnarchuk, S. C. Boehme, S. ten Brinck, C. Bernasconi, Y. Shynkarenko, F. Krieg, R. Widmer, B. Aeschlimann, D. Günther, M. V. Kovalenko, I. Infante, *ACS Energy Lett.* **2018**, *4*, 63.

[38] Q. A. Akkerman, S. G. Motti, A. R. S. Kandada, E. Mosconi, V. D'Innocenzo, G. Bertoni, S. Marras, B. A. Kamino, L. Miranda, F. De Angelis, A. Petrozza, M. Prato, L. Manna, *J. Am. Chem. Soc.* **2016**, *138*, 1010.

[39] S. Jeon, M. C. Jung, J. Ahn, H. K. Woo, J. Bang, D. Kim, S. Y. Lee, H. Y. Woo, J. Jeon, M. J. Han, T. Paik, S. J. Oh, *Nanoscale Horiz.* **2020**, *5*, 960.

[40] B. B. V. Salzmann, M. M. van der Sluijs, G. Soligno, D. Vanmaekelbergh, *Acc. Chem. Res.* **2021**, *54*, 787.

[41] F. D. Ott, A. Riedinger, D. R. Ochsenbein, P. N. Knusel, S. C. Erwin, M. Mazzotti, D. J. Norris, *Nano Lett.* **2017**, *17*, 6870.

[42] S. J. W. Vonk, M. B. Fridriksson, S. O. M. Hinterding, M. J. J. Mangnus, T. P. van Swieten, F. C. Grozema, F. T. Rabouw, W. van der Stam, *J. Phys. Chem. C Nanomater. Interfaces* **2020**, *124*, 8047.

[43] J. Xue, R. Wang, Y. Yang, *Nat. Rev. Mater.* **2020**, *5*, 809.